Effect of a time-dependent magnetic field on the corrosion of nickel-aluminium bronze

Hedda Nordby Krogstad*[a], Roy Johnsen[a] and Michael Coey[b]

[a]*Department of Mechanical and Industrial Engineering, NTNU*
[b]*School of Physics, Trinity College Dublin*
Keywords: Ni-Al Bronze, time-dependent magnetic field, 3.5. wt% NaCl, Thermogalvanic corrosion

[a] MTP Gloeshaugen, Richard Birkelands vei 2B, 7491 Trondheim, Norway
[b] Trinity College Dublin, College Green, Dublin 2, Ireland

*Corresponding author:
Tlf: 0047 906 05 873
Email: hedda.krogstad@ntnu.no.

ABSTRACT

Nickel-aluminium bronze (NAB) was anodically polarized in a solution of 3.5 wt% NaCl and exposed to a time-dependent magnetic field (TDMF) with an amplitude of 180 mT. The effect of a TDMF on the anodic behavior of NAB has been investigated as a function of frequency of the TDMF (0 to150 Hz) and the anodic polarization potential (-180 $mV_{Ag/AgCl}$ to -25 $mV_{Ag/AgCl}$, OCP in the range of -210 $mV_{Ag/AgCl}$). The results show that the anodic current density at a fixed potential increases when NAB is exposed to a TDMF. The effect increases with frequency of the TDMF, and is highest for the lowest polarization potentials. At -180 $mV_{Ag/AgCl}$ the current density increased by 800 % when the sample was exposed to a TDMF of 150 Hz. The increase in current density is explained in terms of joule heating resulting from the induced eddy currents in the NAB sample. The increased anodic reaction at increasing temperature was documented by recording polarization curves at 20°C, 40°C and 60°C. The results emphasize a potential limitation of the use of NAB in close proximity to TDMFs in chloride-containing media.

INTRODUCTION

Nickel-aluminium bronze (NAB) is an alloy often used in heavy duty applications such as pumps, propellers, valves and heat exchangers operating in seawater [1]. A high resistance against corrosion fatigue, good castability, machinability and mechanical properties are the main reasons why NAB is widely used in such applications [2]. These properties also make NAB a good candidate material for the rotor in brushless permanent magnet motors (PMM), or generators, operating in seawater. However, recently reported corrosion of NAB-rotors in seawater-immersed PMMs has cast attention on the alloy's performance in the vicinity of strong, time dependent magnetic fields [3].

Depending on the motor-design, a rotor of a PMM will have permanent magnets embedded on its outer diameter. The rotor is placed inside a concentric stator housing, with a radial clearance (known as the airgap) as small as possible (range of a few mm) [4]. In the stator, insulated copper wires are wound around the stator teeth according to the specific motor design. When voltage is applied to the windings, a dynamic magnetic field is set up in the stator. The interaction between the dynamic magnetic field from the stator and the magnetic field from the permanent magnets produces torque which causes the rotation of the rotor [5].

Ideally, a fixed point on the rotor would "see" the same magnetic flux at all times during rotation, but this is not the case due to two reasons [6]; i) the slotted stator windings, causing uneven distribution of the magnetic flux density in the airgap (i.e. space harmonics) and ii) the nonsinusoidal stator phase current generated by inverter power supply, causing time harmonics [7–9]. The space- and time harmonics seen by the rotor is equivalent to a time-dependent magnetic flux density **B** flowing into the rotor. Faradays law of induction states that a voltage will be induced in conductors when exposed to a time dependent **B**, according to Equation (1):

$$\nabla \times \boldsymbol{E} = -\frac{\partial \boldsymbol{B}}{\partial t} \qquad (1)$$

Where **E** is the electric field in volts, **B** is the magnetic flux density in Tesla and t is time (s). Further, Ohm's law states that the current density **J** (A/m^2) in a conductor will follow Equation (2):

$$\boldsymbol{J} = \sigma \boldsymbol{E} \qquad (2)$$

Where σ is the conductivity of the conductor in S/m. Hence, currents are induced in the rotor of the PMM and circulate in the conductor volume when the motor is running. Since the flow pattern of the

induced currents resembles swirling eddies in a river, they are called eddy currents [10]. Eddy currents are considered a loss is PMMs and causes I^2R heating (i.e. joule heating when current I flows in a conductor with a resistance R), which can be problematic if there is insufficient cooling [5,10]. The primary eddy current loss is in the stator. In an example given in reference [11], the stator loss accounts for 34 % of the total loss in a 4-pole PMM, while the rotor loss stands for 21 %. The eddy current power loss in a conductor is approximately described by the relationship given in Equation (3):

$$P_e = k_e h^2 f^2 B^2 \quad (3)$$

where P_e is the eddy current power loss in W/kg, *h* is the material thickness in the plane perpendicular to the magnetic field, k_e is a material-dependent constant, f is the frequency of applied excitation (Hz), and B is the flux density amplitude within the material in Tesla [5]. The main problem related to heating in PMMs is the risk of overheating of the windings and/or demagnetization of the permanent magnets [12,13]. A safe operating temperature of NdFeB magnets is in the range of ≤ 100°C [14], while the maximum operating range for the windings depends on the insulation class and thermal aging of the winding insulation [13]. To stay in a safe operating temperature range (≤ 100°C) is not a major problem in PMMs operating in seawater, as water is freely flowing at a high rate around the motor and in the "airgap" when the motor is running, providing efficient cooling of both stator and rotor. However, the joule heating of the rotor due to induced eddy currents may have deleterious effects on corrosion, as will be discussed in this paper.

Of special interest in this work is the PMM sketched in FIGURE 1 where the rotor is working as a lateral propeller mounted in the bow of the ship, i.e. a thruster.

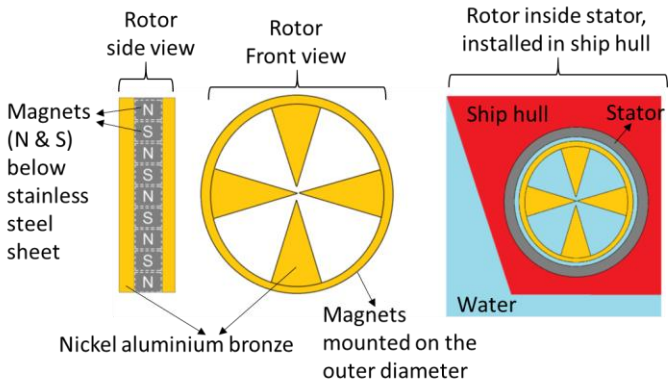

FIGURE 1: Sketch of a PMM designed as a propeller installed in a ship hull. Magnets with alternating poles, north (N) and south (S) facing outwards are mounted on the outer diameter of the rotor, and are protected from the seawater by a stainless steel sheet.

As seen in FIGURE 1 , NAB is used as material in the rotor part of the PMM propeller. On the outer diameter (OD) of the propeller, permanent magnets are embedded into a groove in the NAB. Above the permanent magnets, a stainless steel sheet is mounted flush with the NAB and protects the magnets from exposure to seawater. When the rotor is mounted inside the stator, the copper windings in the stator will be situated above the permanent magnets. The windings have an axial length superior to the axial length of the magnets, and will protrude above the NAB situated directly adjacent to the permanent magnets. In this design, the NAB adjacent to the permanent magnets on the rotor will be a part of the magnetic circuit, and be directly exposed to the TDMF resulting from the space- and time harmonics from the stator windings.

The stainless steel sheet protecting the permanent magnets is a non-magnetic stainless steel (EN 1.4404). Previous work by the author focused on the effect of the galvanic coupling between EN 1.4404 and NAB in natural seawater. It was found that NAB is anodic in the coupling and that galvanic corrosion is limited by the efficiency of the stainless steel cathode. The galvanic current density stabilized at 0.12 A/m^2 for area rations of 1:1 between the NAB and stainless steel in slowly flowing seawater [3]. It is hence established that NAB in the PMM rotor in the design presented in FIGURE 1 is anodically polarized due to galvanic coupling to stainless steel [3]. To investigate the effect of electromagnetic fields on anodically polarized NAB, the topic was divided into two parts: i) effect of a uniform, static magnetic field, and ii) the effect of a time-dependent magnetic field (TDMF). In part one, which will be published in a separate paper,

the effect of the Lorentz force was investigated. The Lorentz force, which acts on moving charges in a magnetic field and induces convection in the electrolyte [15], was found to increase the corrosion current density of anodically polarized NAB by up to 52 % in a magnetic field of 800 mT. In part ii), which is the topic of the work presented in this paper, the goal is to document the effect of a TDMF on the corrosion of anodically polarized NAB.

NAB is an alloy containing about 80 wt.% Cu, and behaves very similarly to unalloyed copper upon immersion in chloride-containing electrolytes such as 3.5 wt.% NaCl solution and natural seawater [16,17]. NAB has a complex microstructure due to the precipitation of several intermetallic particles during cooling from molten state, and reference is given to the book on aluminium bronzes of Harry Meigh for more details [1]. Upon exposure in chloride-containing media, the dominating electrochemical reaction is the dissolution of Cu from the alpha-phase to form $CuCl_2^-$ through the reaction shown in Equation (4) [3,18–21]:

$$Cu + 2Cl^- \rightarrow CuCl_2^- + e^- \quad (4)$$

The anodic reaction at the open circuit potential (OCP) is under mixed charge transfer and mass transport control [17,19,21], meaning that the anodic current will increase both with polarization in the anodic direction, and by increased convection in the electrolyte. The cathodic reaction (oxygen reduction reaction) is under charge transfer control at OCP [17,22].

The effect of temperature on the anodic and cathodic reaction of freshly exposed NAB is of interest for the work presented here. It is expected that both reactions increase with temperature, as natural convection and chemical processes are accelerated by an increase in temperature. Schüssler et al. exposed samples of NAB to synthetic seawater at room temperature and 40°C, and reported a significantly higher initial corrosion rate for the samples exposed to the higher temperature [23].

When a thermal gradient is created in metal exposed to an electrolyte, thermogalvanic corrosion may occur[24]. The driving force is an induced voltage between hot and cold areas [25]. The hot area will normally be electrochemically more active than the colder areas, and will become the anode in the thermogalvanic couple [24]. Boden investigated the effect of thermogalvanic corrosion on pure copper in an aerated 3 wt.% NaCl solution, and found that i) the OCP decreases by 0.6 ± 0.05 mV/°C in the temperature range of 30-60°C, and ii) a substantial thermogalvanic corrosion of pure copper can be established if a hot-spot is created [25]. Relevant thermal properties of NAB are: i) thermal conductivity: 33-46 W/mK and ii) specific heat capacity: 420 J/kgK [1].

NAB used in the PMM propellers contains 4.5-5.5 wt.% Ni and 4.0-5.0 wt.% Fe. Most of the Fe and Ni is found in the intermetallic particles, making the alloy ferromagnetic. The relative magnetic permeability of an equivalent alloy (BS1400-AB2, nominal composition 80Cu 10Al 4.5Fe 5Ni) is between 1.4 and 2 according to Wenschot [26]. Hence, the alloy is attracted to a magnet, and it is magnetized by an external magnetic field. The room-temperature saturation magnetization (M_S) of the alloy used in the experimental work is 28 kA/m [3]. For comparison, the M_S of metallic Fe and Ni are 1 745 and 521 kA/m, respectively [27]. Any effect of hysteresis loss in NAB is not accounted for in this work.

Experimental methods

The composition of the alloy used in the experimental work is provided in Table 1. The alloy is CuAl10Fe5Ni5-C-GS as described in EN 1982:20081. The electrolyte was distilled water with 3.5 wt.% NaCl if not stated otherwise. The electrolyte was not stirred and no air or gas was purged through the solution. All exposed surfaces were ground with 600 grit paper within 5 minutes prior to immersion to the electrolyte. The samples were left 10 minutes in the electrolyte to stabilize at OCP before further electrochemical experiments were conducted. The experiments were performed with a Gamry 2 Interface 1000 potentiostat, and each test was performed at least twice, unless stated otherwise.

[1] EN: European Standard EN 1982:2008, Copper Alloys – ingots and castings

[2] Gamry™ (https://www.gamry.com/potentiostats/interface-1000e-potentiostat/)

Table 1: Composition of the NAB alloy used in the experimental work.

Element	Cu	Al	Fe	Ni	Cr	Mg
wt.%	80.52	9.44	4.23	5.04	<0.005	<0.01
Element	Mn	Pb	Sn	Zn	Si	
wt.%	0.72	<0.01	0.01	0.03	0.02	

The NAB samples were disk-shaped; 28.0 mm in diameter and 2.5 mm thick. The samples were sandblasted and painted with two layers of Jotamastic 87[3], a two-component paint, before polishing one of the disk-surfaces. A stiff stainless steel wire, 1.6 mm in diameter, was inserted into a drilled hole on the rim of the disk and pinched in place (by a strike with a chisel and a hammer) to secure good electrical contact with the test sample. The stainless steel wire was covered by heat-shrink tubing (and silicon at the connection point) to prevent the wire from being exposed to the electrolyte.

Anodic and cathodic polarization curves were recorded on NAB at three different temperatures: 20°C (RT), 40°C and 60°C. To achieve the desired temperature in the electrolyte, the electrolyte container (glass) was placed on a hot plate. A temperature sensor used to automatically maintain the temperature was placed in the electrolyte at the same distance from the hot plate as the center of the NAB sample. A platinum plate (10x10x0.2mm) suspended in a platinum wire was used as counter electrode, and a luggin capillary and salt bridge connected the electrochemical cell to the reference electrode (saturated Ag/AgCl/KCl, referred to as Ag/AgCl from now on). The polarization curves were recorded continuously from -600 to +100 $mV_{Ag/AgCl}$ at a scan rate of 20 mV/min. No repeats were performed.

An aluminium rotor with 24 NdFeB permanent magnets (20x20x10 mm) embedded axially was designed and produced at School of Physics at Trinity College[4]. The magnets were inserted in pockets in the aluminium-frame, with alternating poles facing outwards, and glued with a two-component glue. The rotor, presented in FIGURE 2, had an outer diameter of 215 mm.

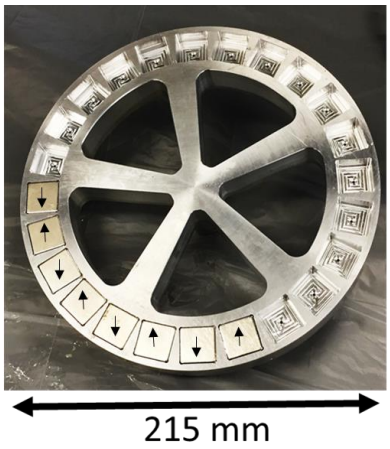

FIGURE 2: The rotor with magnets inserted axially. The picture was taken during production of the rotor, when permanent magnets was inserted and glued into the machined pockets (8 magnets inserted, 16 magnets still missing). The arrows indicate the orientation of the poles.

The rotor was mounted by heat-shrinking onto the shaft of a Leroy Somer[5] LS2 1.5 kW motor. By means of a SEW[6] Eurodrive MOVITRAC® MC07B frequency inverter, the rotation rate of the rotor could be manually adjusted between 0 and 750 revolutions per minute (rpm). During one turn of the rotor, 24 magnets, i.e. 12 pole-pairs, will pass a fixed point in space. Hence, 1 rpm equals a frequency of 12 periods divided by 60 seconds = 0.2 Hz. The experiments were conducted at 0, 200, 400, 600 and 750 rpm, yielding frequencies of 0, 40, 80, 120 and 150 Hz. A plastic container (300x250x60 mm) was custom made to accommodate the test set-up in the experiments where the 24-magnet rotor would be rotated as close as possible to the working electrode. The container was produced from 10 mm thick acryl plates, and fitted with a wooden top with connection points for the working- and counter electrode (platinum wire). The reference electrode (Ag/AgCl) was connected to the test-cell via a silicon tube and a Lugging capillary. An overview of the test set-up is shown in FIGURE 3 a) and b).

[3] Jotamastic from Jotun™ (http://www.jotun.com/we/en/b2b/paintsandcoatings/products/jotamastic-87.aspx)

[4] https://www.tcd.ie/Physics/

[5] http://www.emersonindustrial.com/en-EN/Leroy-Somer-Group/Pages/home.aspx

[6] http://www.seweurodrive.com/

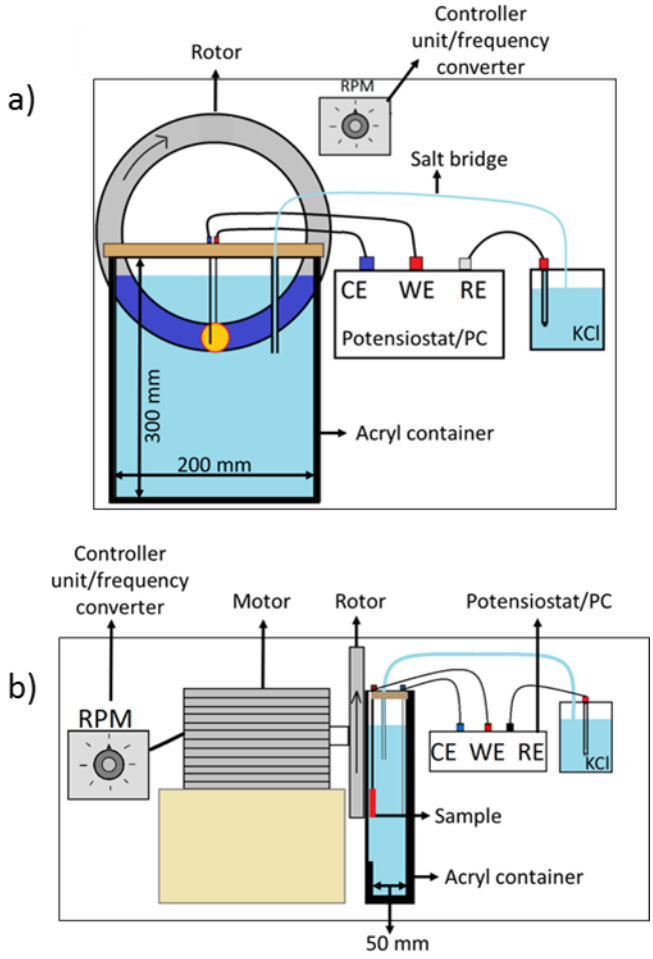

FIGURE 3: Sketch of the set-up with the rotor placed close to the sample surface. Front-view in a), side-view in b). Notice the difference in the acryl container thickness on the side facing the rotor in b). CE, WE and RE refer to counter, working and reference electrodes.

In order to reduce the total distance between the rotor magnets (on the outside of the container, in air) and the exposed sample surface (inside the container, in the electrolyte), a part of the acryl wall was cut away and replaced by a 1 mm thick acrylic sheet. The sample was mounted so that the coated side was facing the rotor magnets and as close as possible to the 1 mm acryl sheet. With this set-up, the total distance between the surface of the rotor magnets and the exposed NAB surface was 4 mm. The magnetic field intensity on the sample surface when each of the 24 rotor-magnets was placed directly behind the sample, was measured with a gaussmeter (Hirst Instruments GM07[7]). The average value and standard deviation was 179 ± 6.4 mT (positive poles), and -183 ± 8.1 mT (negative poles). Hence the average amplitude of the TDMF was 181 mT on the exposed surface of the NAB sample

To investigate the effect of different frequencies of TDMF on: i) OCP and ii) the current density on anodically polarized samples, different rotation rates for the rotor were used during the experiments. At the beginning of each experiment, the rotor was turned off and kept at a distance away from the acryl container, as any interaction with the static magnetic field and the sample was unwanted. After an initial period of 10 minutes, the rotor was set to rotate at 200 rpm, and moved towards the sample, as close as possible without colliding with the acryl container (~0.5mm). The rotation rate of the rotor was further increased after 3 minutes to 400, 600 and 750 rpm. At each rotation rate, the holding-time was 2 minutes, hence the time vs. rotation rate/frequency was according to FIGURE 4. The reason for 3 minutes holding time at 200 rpm was that it took approximately 1 minute to manually move the rotor in position next to the acryl container. In the potentiostatic polarization experiments, five anodic potentials were chosen: -180, -130, -90, -50 and -25 $mV_{Ag/AgCl}$ (OCP was in the range of -210 ± 10 $mV_{Ag/AgCl}$). The current density was measured as a function of time and frequency of the TDMF.

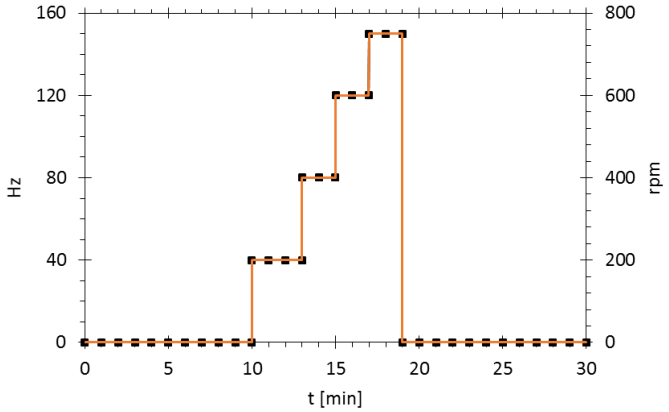

FIGURE 4: Rotation rate of the rotor as a function of time in the electrochemical experiments where the TDMF was applied.

The temperature on the exposed (i.e. uncoated) surface of the NAB sample was measured as a function of rotation rate by means of a thermocoupl[8]. The junction between the two dissimilar metal wires of the thermocouple was ball-shaped, 1 mm in diameter. The "ball" was placed in the center of the exposed surface of the NAB sample during the

[7] http://www.hirst-magnetics.com/instruments/gm07_p1.shtml

[8] Standard lab-equipment, reference is made to "Manual on the Use of Thermocouples in Temperature Measurement" [30].

temperature measurements, in metallic contact with the sample. The sample and thermocouple was immersed in the electrolyte, and the rotor rotated according to the description in FIGURE 4. One repeat of temperature measurement was conducted while simultaneously measuring the OCP of the NAB sample. The rotor only rotated at one speed (60 rpm, i.e. TDMF of 120 Hz) during this experiment.

Two NAB samples were freely exposed at OCP for four weeks in fresh, natural seawater at 11±2°C to obtain an aged condition. The seawater was taken from the Trondheim fjord at 80 m depth and circulated continuously at a rate of 0.001 m/s in a 160L tank. After four weeks of exposure, the two samples were potentiostatically polarized to -50 $V_{Ag/AgCl}$ in the acryl container and exposed to the TDMF described in FIGURE 4. Natural seawater from the Trondheim fjord at room temperature was used as electrolyte during the experiments with the TDMF on the aged samples.

The induced eddy currents and the loss related to joule heating due to a TDMF were calculated by modelling using Comsol Multipysics[9]. The problem was simplified to the NAB sample and *one* magnet, solving Maxwell's equations in the frequency domain. The induced eddy currents and power loss was calculated at 40, 80, 120 and 150 Hz. The sample and magnet were sketched to real size, and with 4 mm separation, as in the lab-set up. The remanent magnetization of the permanent magnet was set to 0.4 T, and the relative permeability and conductivity of NAB was set to 1.4 and $7.7x10^6$ S/m, respectively. To help the 3D model converge, the electrical conductivity of air, electrolyte and acryl container was set to 100 S/m, and for *all* materials, the relative permittivity was set to 1.0.

Thermogalvanic corrosion tests were conducted with two NAB samples exposed to the electrolyte in the acrylic container; one sample was placed in the 'normal' configuration, i.e. close to the magnets of the rotor, while the second sample was placed 5 cm below the path of the magnets, see FIGURE 5. A voltmeter was used to measure the potential and the current (across a 10 Ohm resistor) between the samples. The voltage drop across the resistor was transferred to current via Ohm's law. Two repeats were performed for each test.

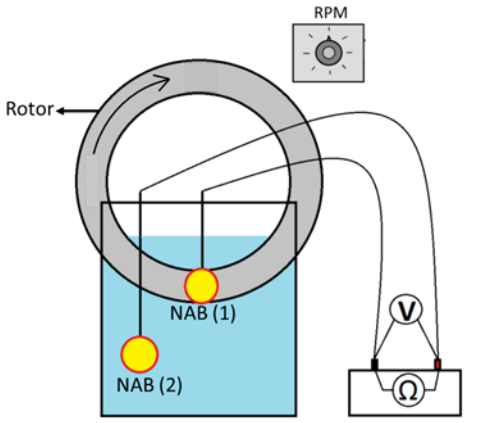

FIGURE 5: Thermogalvanic corrosion experiment. Galvanic current measured as a potential drop (V) across a known resistor (Ω).

Experimental results and discussion

FIGURE 6 shows the polarization curves recorded on NAB at three different temperatures. The curves are shown in the potential range from -400 to 0 $mV_{Ag/AgCl}$, considered as the most relevant potential range in this work.

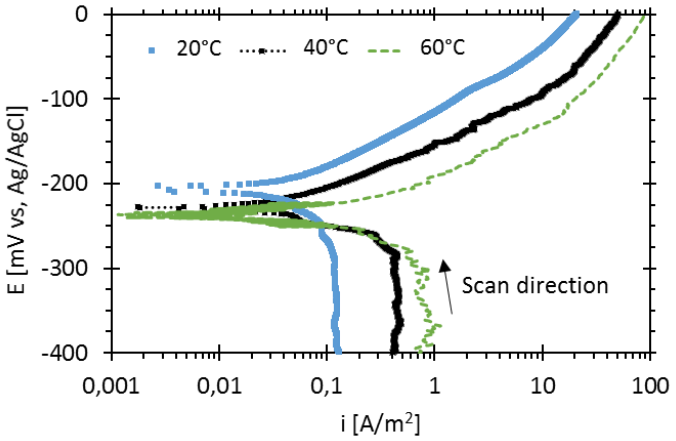

FIGURE 6: Polarization curves recorded on NAB in a 3.5 wt% NaCl solution. The scan rate was 20 mV/min.

The anodic and cathodic curves shift towards lower OCP and higher current densities at a fixed potential with increasing temperature. Extrapolating the anodic curves to OCP yields approximate corrosion current densities of 0.04, 0.05 and 0.175 A/m^2 at 20°C, 40°C and 60°C, respectively. Decreasing OCP and increasing anodic currents with increasing temperature is in accordance with the work of Boden [25] and Schüssler[23]. The cathodic curves are characterized by a higher limiting current, and by a narrower region of charge-transfer control, with increasing temperature. The anodic curve is characterized by similar tafel slopes in the apparent tafel region, but a

[9] Trade mark

significant increase in current density at a given potential. As an example: at -50 $mV_{Ag/AgCl}$, the anodic current density is: 8, 25 and 50 A/m^2 in 20°C, 40 °C and 60°C, respectively. This corresponds to a relative increase in current density of 212 % and 525 % for 40°C and 60°C relative to 20°C. At -180 $mV_{Ag/AgCl}$, the equivalent values for the relative increase in current density at 40°C and 60°C compared to 20°C are 215 % and 1 494 %. This shows that a rise in temperature will have the highest relative impact on current density at low overpotentials from OCP/low anodic current densities.

The effect of a TDMF on OCP of NAB is presented in FIGURE 7. It is a clear trend that OCP drops when a TDMF is applied, and continues to decrease with increasing frequency. When the TDMF is turned on (to 40 Hz), the OCP drops from -204 $mV_{Ag/AgCl}$ to -212 $mV_{Ag/AgCl}$, i.e. 8 mV. When the TDMF is turned off (from 150 Hz), the OCP raises from -217 $mV_{Ag/AgCl}$ to -206 $mV_{Ag/AgCl}$, i.e. 11 mV. The results were repeatable, with a decrease and increase of 7 mV and 10 mV when turning on (to 40 Hz) and off (from 150 Hz) the TDMF, respectively, in the 2nd repeat.

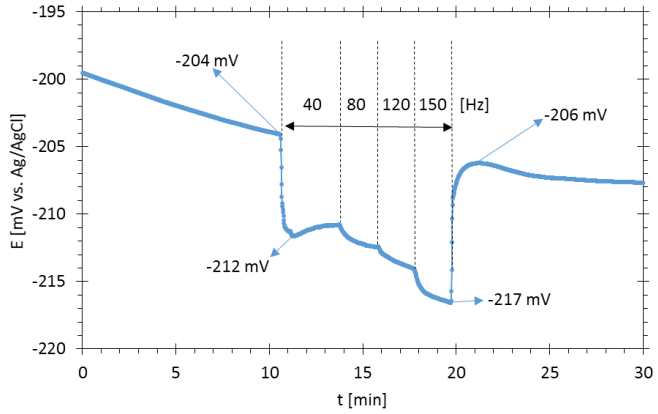

FIGURE 7: OCP measured on NAB during 30 minutes of exposure to 3.5 wt% NaCl at room temperature. The TDMF variation was 40, 80, 120 and 150 Hz as indicated on the figure. Reference is made to the time vs. frequency diagram in FIGURE 4.

The effect of a TDMF on the current density during potentiostatic polarization to selected anodic potentials are presented in FIGURE 8. Both repeats are presented for each polarization potential. The anodic current density increases with increasing frequency, and is higher than in the absence of a TDMF at polarization potentials of -180, -130 and -90 $mV_{Ag/AgCl}$ (FIGURE 8 a-c). For the samples polarized to -50 $mV_{Ag/AgCl}$ (FIGURE 8 d) and -25 $mV_{Ag/AgCl}$ (FIGURE 8 e), the current density decreases when the TDMF is turned on at 40 Hz, but then increases above the level recorded just before the onset of the TDMF when the frequency is increased to 80 Hz. Electromagnetic noise was induced to the electrochemical measurements when the TDMF was applied. The noise with respect to the measured current density was significant at the most negative polarization potentials (i.e. -180 and -130 $mV_{Ag/AgCl}$), observed by the wide spread in measured current density in FIGURE 8 a) and b). When the TDMF was turned off, however, the curves stabilized immediately, and always from the highest values recorded. The highest values of current density at each potential are therefore used as reference values in the following discussion.

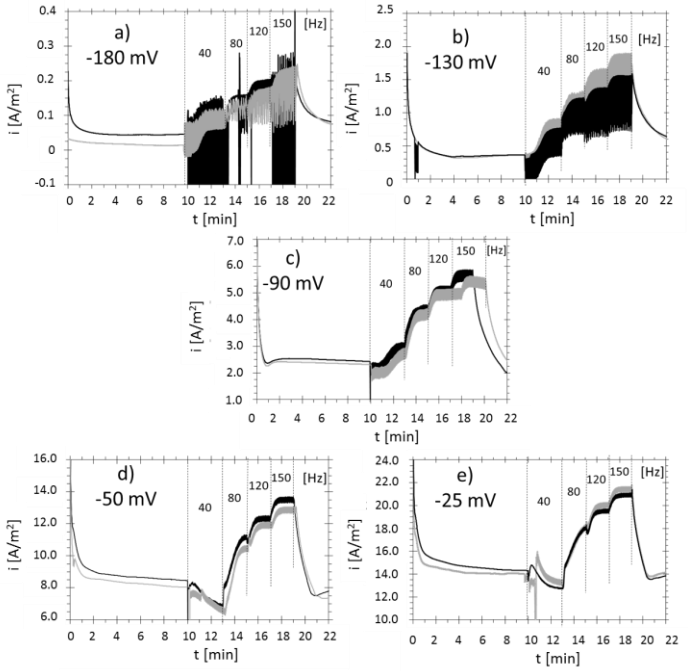

FIGURE 8: Potentiostatic polarization of NAB to five different anodic potentials as indicated in a)-e). All potentials are with respect to Ag/AgCl. After 10 minutes a TDMF is applied with the sequence presented in FIGURE 4: 40, 80, 120 and 150 Hz. Both repeats are shown for each potential.

When the rotor was turned on during the potentiostatic polarization experiments, the potentiostat software notified a control amplifier overload (CA OVLD), indicating that the potentiostat cannot supply enough current between working and counter electrodes to reach the desired potential at the working electrode [10]. This is attributed to electromagnetic noise when the rotor was turned ON. The recorded polarization potential during the time

the rotor was turned on was lower than the set potential on the potentiostat, and was not affected by the rotation rate of the rotor. The potential vs. time recorded by the potentiostat is presented in FIGURE 9. The values of set potential and the corresponding measured potentials are tabulated in Table 2.

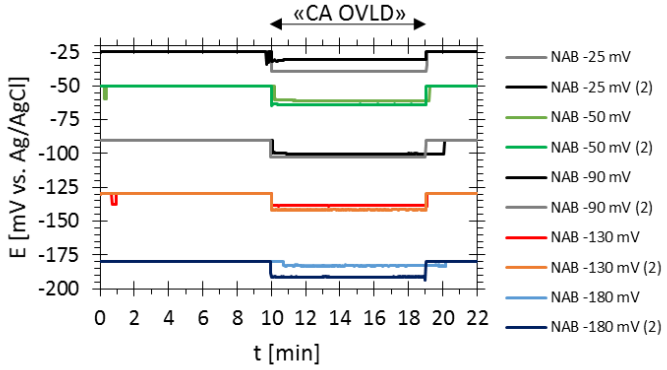

FIGURE 9: Potential of NAB exposed to a TDMF as recorded by the potentiostat during potentiostatic polarization and exposure to TDMF. The TDMF was applied in the region were the potential deviates from the set potential, where the potentiostat software signaled 'CA OVLD'.

Table 2: The set potentials and measured potential recorded during potentiostatic experiments with the rotor turned ON. Potentials are with respect to the Ag/AgCl reference electrode.

Set potential [mV]	Recorded potential w/rotor ON [mV]	
	1st repeat	2nd repeat
-25	-39	-31
-50	-61	-64
-90	-100	-103
-130	-142	-139
-180	-183	-192

The significance of the electromagnetic noise with respect to the validity of the experiments is a point of interest. As the electromagnetic noise from the TDMF appears to reduce the actual polarization potential, it becomes less meaningful to compare the current densities recorded with and without the TDMF applied, as they are with respect to two different potentials. However, this has been done in the following discussion, and the results should only be regarded as useful for *comparison*. Regarding elimination of the electromagnetic noise, the source of the noise is the rotating rotor, and therefore not possible to remove.

The results in FIGURE 8 are presented as average current density versus frequency in FIGURE 10 a). In FIGURE 10 b) the results are plotted as average relative increase in current density vs. the average current density measured after 10 minutes (i.e. just before the onset of the TDMF). It is clear that with higher initial current densities (i.e. higher polarization potential), the relative increase in current density becomes less significant. The maximum increase in current density occurred for the samples polarized to the lowest anodic potential (-180 $mV_{Ag/AgCl}$), where the average current density was 0.02-0.03 A/m^2 in the absence of a TDMF, while it increased by 800 % when a TDMF of 150 Hz was applied, see FIGURE 10 b). If a temperature-increase in the sample resulting from eddy currents and joule heating is responsible for the increase in current density, the results are in good accordance with the polarization curves in FIGURE 6, where the relative effect of increasing temperature was highest close to the OCP.

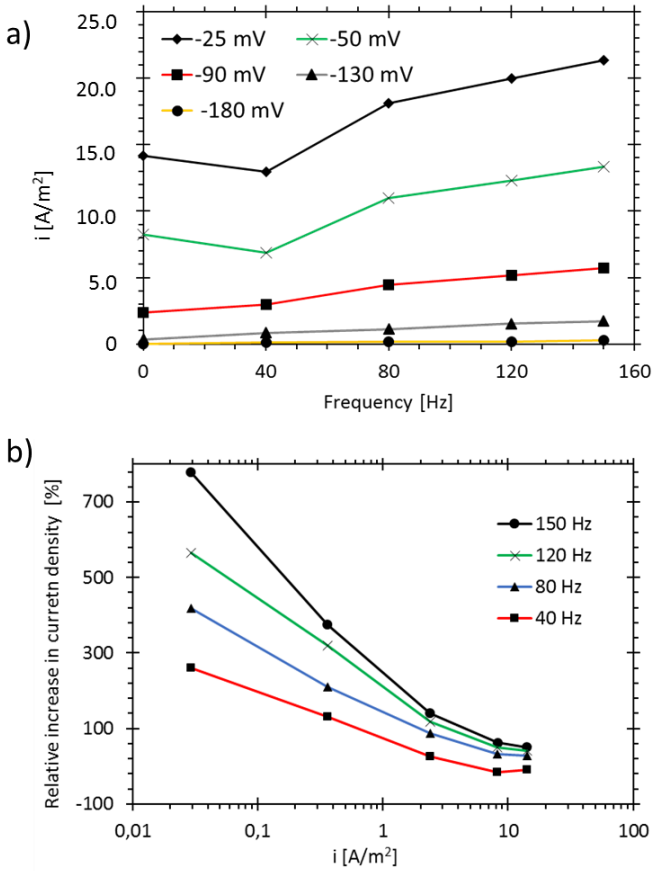

FIGURE 10: In a) the average current density as a function of frequency of the TDMF and polarization potential. In b) the relative increase in current density as a function of initial current density and frequency of the TDMF. Potentials are with respect to the Ag/AgCl reference electrode.

The aged samples, kept four weeks in natural seawater prior to the test with TDMF, had a much lower current density after 10 min of polarization to -50 $mV_{Ag/AgCl}$ than the "fresh" samples; i.e. 0.215 A/m^2

(see FIGURE 11) compared to ~ 8 A/m^2 (ref. FIGURE 8 d). This is due to formation of a passive film on the surface of the aged samples through precipitation of solid CuCl and further formation of an aluminium- and copper oxide [3,16,23]. At the onset of the TDMF, the current density of one of the repeats (grey curve in FIGURE 11) had a very large scatter, and the current density during the time the TDMF was ON is not shown for this sample. The relative increase in current density (based on only the black curve in FIGURE 11) was: 5 %, 10 %, 28 % and 43 % for 40, 80, 120 and 150 Hz, compared to the current density right before the onset of the TDMF, respectively. The average values of relative increase in current density at the same frequencies for the fresh samples were -17 %, 33 %, 49 %, and 62 %. This shows that aged NAB also is affected by a TDMF when anodically polarized.

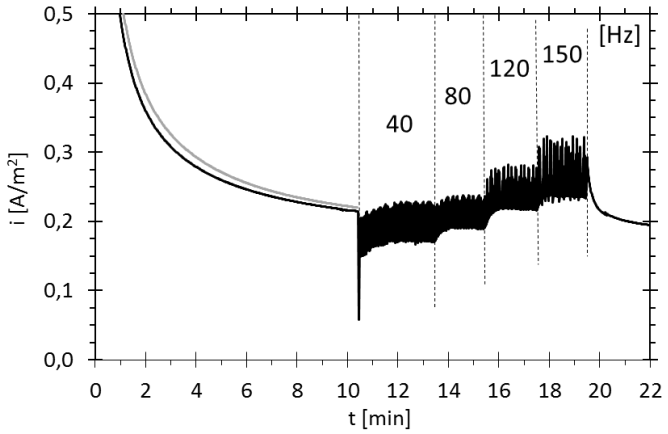

FIGURE 11: Potentiostatic polarization of aged NAB to -50 mV$_{Ag/AgCl}$ with a TDMF applied from the 10th minute.

The temperature measured on the exposed NAB surface (freshly exposed samples) is presented in FIGURE 12. The temperature dropped when the TDMF was turned on (40 Hz). The sudden drop is attributed to electromagnetic noise induced by the TDMF. However, a temperature increase can be extracted from plotting the relative increase in temperature during the 8 minutes the TDMF was turned on, see FIGURE 12 b). The shape of the curves in FIGURE 12 b) resembles those in FIGURE 8, i.e. current density and temperature develops in a similar way with respect to time under the influence of a TDMF. The temperature measured on the sample surface increased by a total of 3.5°C during exposure to the TDMF.

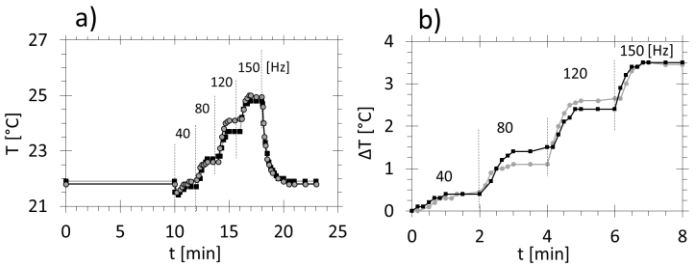

FIGURE 12: a) Temperature measured by the thermocouple situated at the center of an exposed NAB surface while immersed in 3.5 wt% NaCl solution and exposed to a TDMF with a frequency as indicated in the figure. Both repeats are presented. In b) the temperature increase plotted as the temperature *difference (ΔT)* during the 8 minutes the TDMF was applied.

FIGURE 13 shows the correspondence between OCP and temperature when the rotor rotates at 60 rpm, i.e. 120 Hz. The measured temperature also dropped when the TDMF was applied, and the temperature is there for plotted as temperature difference (ΔT). The shape of the two curves have significant similarity, but are opposite to each other: i.e. the temperature increases and the OCP decreases with the same rate when the TDMF is turned on. The total increase in temperature was 3.5°C and the total change in OCP was 15 mV, indicating a temperature-dependent change in potential of NAB by 4.3 mV/°C. This is significantly higher than that reported on pure Cu (0.6 mV/°C)by Boden [25].

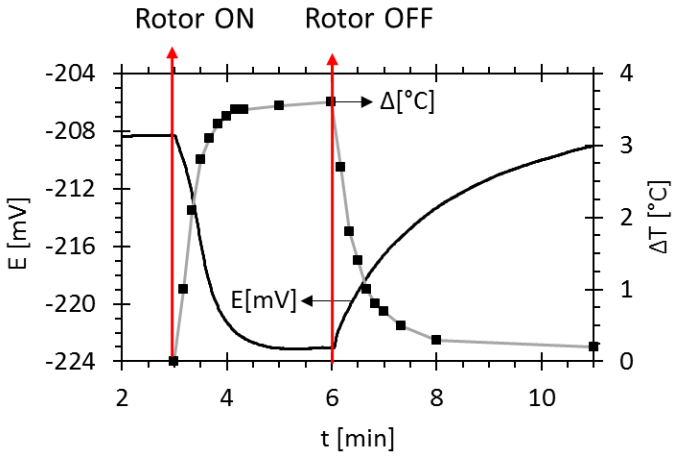

FIGURE 13: OCP and temperature of NAB in a 3.5 wt.% NaCl solution with a TDMF with a frequency of 120 Hz turned on/off after 3 and 6 minutes. Potentials are with respect to the Ag/AgCl reference electrode.

The results presented in FIGURE 8, FIGURE 12 and FIGURE 13 suggests that it is the rise in temperature of the NAB sample (resulting from the induced eddy currents and joule heating) that is responsible for the increase in current density at a fixed potential and the

decrease in OCP when a TDMF is applied. The increase in current density resulting from the rising temperature more than compensates for the decrease in current density related to the electromagnetic noise and lower effective polarization potential (ref. FIGURE 9 and Table 2) for all potentials/frequencies except for the highest polarization potentials (-25 and -50 $mV_{Ag/AgCl}$) and the lowest frequency (40 Hz), ref. FIGURE 8. For these combinations of potentials/frequency, the reduction in current density related to a lower polarization potential was greater than the increase in current density related to rising temperature of the sample. However, as the increase in current density due to rising temperature of the sample increases with the frequency of the TDMF, while the effective polarization potential was constant and independent of frequency (ref. FIGURE 9), it is expected that a net increase in current density is observed with higher frequencies. Indeed, at 80 Hz, all potentiostatic tests showed a net increase in current density relative to the value recorded just before the onset of the TDMF, ref. FIGURE 8. In conclusion, the results highly indicate that a TDMF will increase the current density of anodically polarized NAB, by increasing the temperature of the sample and thereby accelerating the anodic reaction.

The results from the thermogalvanic test are presented in

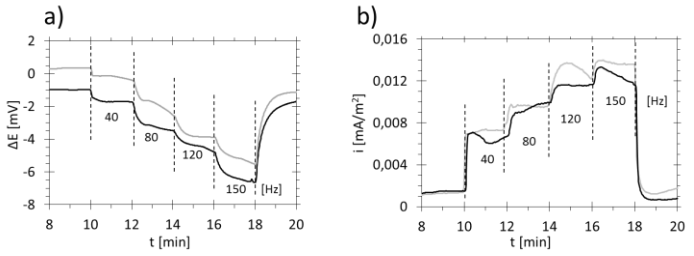

FIGURE 14. The potential difference between NAB1 and NAB2 (ref. FIGURE 5) increases in magnitude as a function of TDMF frequency, and at 150 Hz the potential between the samples have changed by 5.75 mV (average value of the two repeats). This is lower than the change in OCP found on one single NAB sample exposed to the same TDMF (11 mV), see FIGURE 7. The galvanic current between NAB1 and NAB2 was initially 0.001 A/m^2 and increased as a function of frequency of the TDMF, reaching a maximum 0.13 and 0.014 A/m^2 in the two repeats at 150 Hz, see

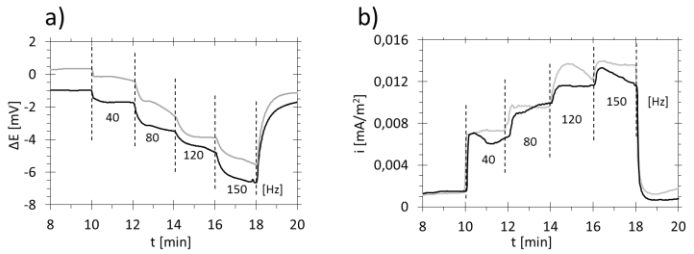

FIGURE 14 b). A positive current indicates that NAB1 (the sample placed adjacent to the rotor) is the anode. The results in

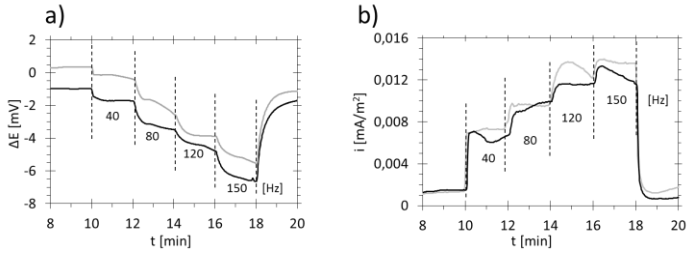

FIGURE 14 show that NAB suffers thermogalvanic corrosion when only one sample is exposed to a TDMF, and that the galvanic current density increases with increasing frequency of the TDMF.

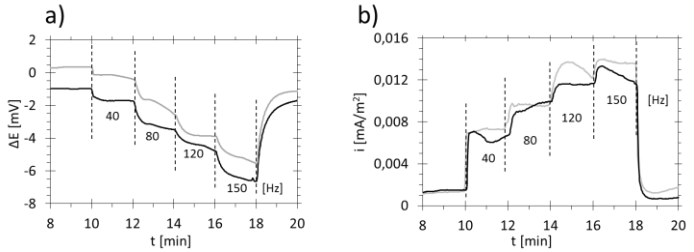

FIGURE 14: a) Potential difference between NAB1 and NAB2 in the thermogalvanic experiment (ref. FIGURE 5) when NAB1 is exposed to a TDMF of different frequencies. b) Current density recorded between NAB1 and NAB2 when NAB1 is exposed to a TDMF of different frequencies. Both repeats are presented.

The results from modelling the induced eddy currents in the NAB sample exposed to a TDMF of 40, 80 120 and 150 Hz are presented as color-maps and arrows in FIGURE 15 a). The induced current density is lowest in the origin, and increases with the radius of the sample and with frequency. A cross section of the sample, with colors indicating the volumetric loss in W/m^3 is presented in FIGURE 15 b). It is clear that the NAB surface facing the magnet generates more loss than the exposed NAB surface. However, the thermal conductivity of NAB will contribute to a more uniform temperature distribution in the sample volume. The power loss (W) for the whole sample at each

frequency was found by integrating, and the result is plotted in FIGURE 16. Multiplying the power loss (W) by the time-period the sample was exposed to each frequency (120 s) yields the accumulated loss at each frequency (J). This is plotted on the secondary y-axis in FIGURE 16. Adding together the accumulated loss at each frequency yields a total of 98.3 J during the period the rotor is spinning next to the sample (8 min). In theory, 98.3 Joule can increase the temperature of the NAB sample by 20°C (based on the specific heat capacity of 420 J/kgK and a density of 7.5 g/cm^3, values taken from reference [1]). However, as the sample is located in water, cooling of the sample is more efficient than in air, and the temperature increase is less than the theoretical value. The eddy current loss increases exponentially with the frequency of the TDMF, in accordance with Eq. (3).

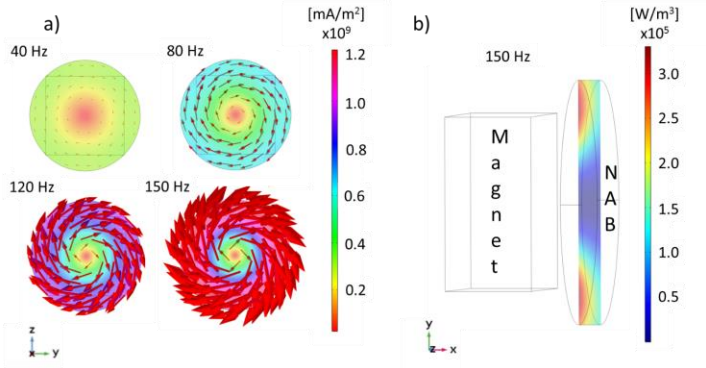

FIGURE 15: Eddy currents induced in the NAB sample as a result of the TDMF of different frequencies. In a) Eddy current density in the plane of the exposed NAB surface presented as colour-scale and arrows. In b) a cross section showing the volumetric loss density in the NAB sample in the plane perpendicular to the permanent magnet in a TDMF of of 150 Hz.

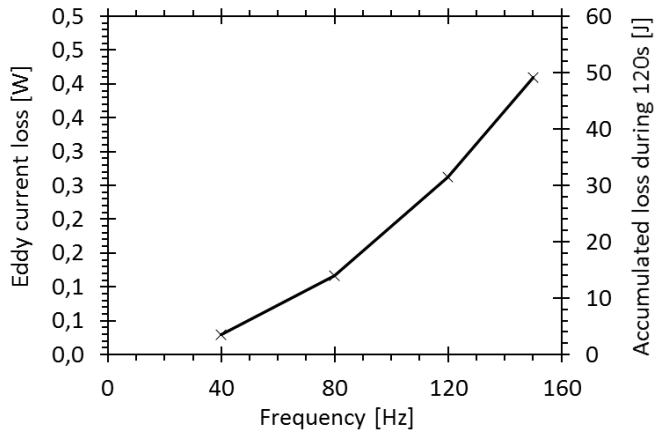

FIGURE 16: Eddy current loss at each frequency (left axis), and total eddy current loss based on 120s of exposure to the TDMF at each frequency (right axis).

The results presented in this work emphasize a possible limitation in the use of NAB in regions exposed to a TDMF. The interactions between the TDMF and the alloy causes joule heating, which renders the alloy more active in terms of corrosion. NAB is also susceptible to thermogalvanic corrosion, which may occur if parts of a larger component of NAB is locally subjected to a TDMF. In terms of the PMM design presented in FIGURE 1, where the NAB is additionally polarized by galvanic coupling to stainless steel, the situation may become severe as the anode surface area will potentially be much less than the cathode surface area. When the PMM is running, seawater will flow at a high rate through the airgap, providing cooling. However, the joule heating will be generated in the metal, and on the NAB surface there will be narrow layer of electrolyte with a temperature gradient. The high flow of the seawater may also yield higher galvanic corrosion rates (both the thermogalvanic and dissimilar metal corrosion) as high flow rates are known to increase the cathode limiting current by increasing the mass transport of oxygen [28,29]. Joule heating and thermogalvanic corrosion, together with the contributions from dissimilar metal corrosion, may have played an important role in causing the corrosion damage observed in the field on the immersed PMMs sketched in FIGURE 1.

Conclusions

- When NAB is exposed to a time-dependent magnetic field of 40-150 Hz, eddy currents are induced, and the metal is heated due to joule heating.
- Polarization curves of NAB recorded at 20°C, 40°C and 60°C show a clear trend of decreasing OCP and higher anodic current densities with increasing temperature.
- The OCP of NAB decreases when a time-dependent magnetic field is applied. A total difference of 11 mV was documented in this work in a field of 150 Hz. The decrease in OCP is correlated to the increase in temperature of the sample.
- Anodically polarized NAB, both freshly prepared and aged samples, suffers higher dissolution rates when a TDMF is applied. The effect, in terms of relative increase in current density, is larger at low

overpotentials. The effect is attributed to the increase in temperature, causing an acceleration of the anodic reaction.

- A maximum increase in current density of 800 % was documented in this work, for a sample polarized to -180 $mV_{Ag/AgCl}$ while exposed to a TDMF of 150 Hz.
- NAB can suffers thermogalvanic corrosion when a "hot spot" arises due to local exposure to a TDMF and related joule heating. The galvanic current density increases with the frequency of the TDMF and reached 0.012 A/m^2 at a frequency of 150 Hz.
- The results indicate that the performance of NAB in rotors of permanent magnet motors operating in seawater might be inadequate when NAB is directly exposed to the time-dependent magnetic field residing from the time- and space harmonics from the stator windings.

References

[1] H. Meigh, Cast and Wrought Aluminium Bronzes, 2000.

[2] I. Richardson, C. Powell, Guide to Nickel Aluminium Bronze for Engineers Guide to Nickel Aluminium Bronze for Engineers, Copp. Dev. Assoc. Publ. No 222. (2016).

[3] H.N. Krogstad, R. Johnsen, Corrosion properties of nickel-aluminium bronze in natural seawater - Effect of galvanic coupling to UNS S31603, Corros. Sci. 121 (2017) 43–56. doi:10.1016/j.corsci.2017.03.016.

[4] A. Judge, Air gap elimination in permanent magnet machines, Worcester polytechnic institute, 2012.

[5] D. Hanselman, Brushless Permanent Magnetic Motor Design, 2nd ed., The Writer's Collective, Cranston, 2003.

[6] J.R. Hendershot, T.J.E. Miller, Design of brushless permanent magnet motors, Magna physics publishing and Clarendon press, Oxford, 1994.

[7] B. Li, M. Li, Calculation and Analysis of Permanent Magnet Eddy Current Loss Fault with Magnet Segmentation, Math. Probl. Eng. 2016 (2016). doi:10.1155/2016/7308631.

[8] F. Deng, Commutation-caused eddy-current losses in permanent-magnet brushless DC motors, IEEE Trans. Magn. 33 (1997) 4310–4318. doi:10.1109/20.620440.

[9] A.K. Nagarkatti, O.A. Mohammed, N.A. Demerdash, Special Losses in Rotors of Electronically Commuted Brushless DC Motors Induced by Non-Uniformly Rotating Armature MMFS, IEEE Trans. Power Appar. Syst. PAS-101 (1982) 4502–4507.

[10] H.D. Young, R.A. Freeman, F. Sears, M. Zemansky, University Physics, 12th ed., Pearson Education, San Fransisco, 2008.

[11] A. Bonnett, C. Yung, Increased Efficiency Versus Increased Reliability, IEEE Ind. Appl. Mag. 14 (2008) 29–36. doi:10.1109/MIA.2007.909802.

[12] T. Miller, Brushless permanent -magnet motor drives, Power Eng. (1988) 55–60.

[13] C. Kral, A. Haumer, S. Bin Lee, A practical thermal model for the estimation of permanent magnet and stator winding temperatures, IEEE Trans. Power Electron. 29 (2014) 455–464. doi:10.1109/TPEL.2013.2253128.

[14] H.B. Ertan, M.Y. Üçtuğ, R. Colyer, A. Consoli, eds., Modern Electrical Drives, Springer Netherlands, Dordrecht, 2000. doi:10.1007/978-94-015-9387-8.

[15] L.M.A. Monzon, J.M.D. Coey, Magnetic fields in electrochemistry: The Lorentz force. A mini-review, Electrochem. Commun. 42 (2014) 38–41. doi:10.1016/j.elecom.2014.02.006.

[16] S. Neodo, D. Carugo, J.A. Wharton, K.R. Stokes, Electrochemical behaviour of nickel–aluminium bronze in chloride media: Influence of pH and benzotriazole, J. Electroanal. Chem. 695 (2013) 38–46. doi:10.1016/j.jelechem.2013.02.007.

[17] G. Kear, B.D. Barker, K. Stokes, F.C. Walsh, Flow influenced electrochemical corrosion of nickel aluminium bronze - Part II. Anodic polarisation and derivation of the mixed potential, J. Appl. Electrochem. 34 (2004) 1235–1240. doi:10.1007/s10800-004-1758-1.

[18] B. Yuan, C. Wang, L. Li, S. Chen, Investigation of the effects of the magnetic field on the anodic dissolution of copper in NaCl solutions with holography, Corros. Sci. 58 (2012) 69–78. doi:10.1016/j.corsci.2012.01.005.

[19] J.A. Wharton, R.C. Barik, G. Kear, R.J.K. Wood, K.R. Stokes, F.C. Walsh, The corrosion of

nickel-aluminium bronze in seawater, Corros. Sci. 47 (2005) 3336–3367. doi:10.1016/j.corsci.2005.05.053.
[20] M.M. Al-Abdallah, a. K. Maayta, M. a. Al-Qudah, N. a. F. Al-Rawashdeh, Corrosion Behavior of Copper in Chloride Media, Open Corros. J. 2 (2009) 71–76. doi:10.2174/1876503300902010071.
[21] G. Kear, B.D. Barker, F.C. Walsh, Electrochemical corrosion of unalloyed copper in chloride media-a critical review, Corros. Sci. 46 (2004) 109–135. doi:10.1016/S0010-938X(02)00257-3.
[22] G. Kear, B.D. Barker, K. Stokes, F.C. Walsh, Flow influenced electrochemical corrosion of nickel aluminium bronze - Part I. Cathodic polarisation, J. Appl. Electrochem. 34 (2004) 1235–1240. doi:10.1007/s10800-004-1758-1.
[23] A. Schüssler, H.E. Exner, The Corrosion of Nickel-Aluminium Bronze in Seawater-I. Protective Layer Formation and the Passivation Mechanism, Corros. Sci. 34 (1993) 1793–1802.
[24] E. Bardal, Corrosion and protection, Springer, 2004. https://www.bokklubben.no/SamboWeb/produkt.do?produktId=1394900 (accessed July 6, 2017).
[25] P.J. Boden, Corrosion of Cu and Cu-base alloys under conditions of boiling heat transfer—I. Corrosion of Cu, Corros. Sci. 11 (1971) 353–362. doi:10.1016/S0010-938X(71)80118-X.
[26] P. Wenschot, A new nickel-aluminum bronze alloy with low magnetic permeability, Metall. Mater. Trans. A. 28 (1997) 689–697. doi:10.1007/s11661-997-0055-0.
[27] H. Danan, A. Herr, J.P. Meyer, New Determinations of the Saturation Magnetization of Nickel and Iron, J. Appl. Phys. 39 (1968) 669–670. doi:10.1063/1.2163571.
[28] G. Hinds, J.N.G. Thomas, The Electrochemistry of Corrosion, Natl. Phys. Lab. (2014). doi:10.1149/1.3494016.
[29] C. Song, J. Zhang, Electrocatalytic Oxygen Reduction Reaction, in: PEM Fuel Cell Electrocatal. Catal. Layers Fundam. Appl., c, 2008: pp. 89–129. doi:10.1007/978-1-84800-936-3_2.
[30] ASTM Committee E-20, Manual on the Use of Thermocouples in Temperature Measurement, (1981). doi:10.1520/STP470B-EB.